Regional and Global-Scale LULC Mapping by Synergetic Integration of NDVI From Optical Data and Degree of Polarization From SAR Data

Geba Jisung Chang, Yisok Oh, *Life Fellow, IEEE*, and Maxim Shoshany

***Abstract*—This study presents a novel classification model, the Normalized Difference Vegetation Index (NDVI), degree of polarization (DOP), texture classification model (NDTCM), for both regional and global scales, utilizing a synergistic approach that combines the NDVI from optical data with the DOP and its associated texture from synthetic aperture radar data. This integration effectively enhances land use and land cover (LULC) mapping. Specifically, Multi-date Moderate Resolution Imaging Spectroradiometer/Landsat images for NDVI extraction and dual polarization Phased-Array L-band Synthetic Aperture Radar data for DOP are employed in this study. This integration enables the NDTCM to effectively classify land cover into five categories: forest, shrubland, urban, cultivated land, and bare surface. Applied to Mediterranean land cover mapping, the NDTCM achieved high accuracy, with rates of 93.3% for forests, 57.5% for shrublands, 64.4% for urban areas, 76.8% for cultivated lands, and 92.8% for bare surfaces. Compared with global land-cover models, such as GlobCover, the NDTCM showed superior performance in forest and shrubland classification, exceeding GlobCover's accuracy of 84.3% for forests and 35.4% for shrublands, in this study case. The contribution of each data source to the classification results was significant. NDVI data were instrumental in identifying vegetative cover. The DOP and texture information enriched the model's capability to discern land cover types by providing insights into the physical structure and heterogeneity of the surfaces, critical for distinguishing between different land covers, such as forest and shrubland. This comprehensive integration demonstrates the NDTCM's potential as a robust framework for future advancements in LULC mapping and environmental studies.**

***Index Terms*—Degree of polarization (DOP), land use land cover (LULC), Mediterranean, Normalized Difference Vegetation Index (NDVI), Phased-Array L-band Synthetic Aperture Radar (PALSAR), texture.**

I. Introduction

LAND use and land cover (LULC) classification plays a vital role in various geo-informational applications, such as monitoring air–surface energy exchange, carbon emissions, observing agricultural and natural ecosystems, and charting land-use transformations, and is becoming increasingly critical at both regional and global scales [1]. As part of the broader effort in LULC analysis, a range of global databases focused on land cover classification maps is consistently maintained. For example, forest/nonforest (FNF) classification employs a 25-m spatial resolution to distinguish forest areas from nonforest ones, providing detailed insights into forest cover dynamics [2]. In contrast, GlobCover09 offers a broader view with its 300-m spatial resolution, categorizing the Earth's surface into 22 distinct cover types ranging from urban areas to various natural landscapes [3], and GlobeLand30 provides a finer granularity with a 30-m resolution, focusing on nine key land-cover categories, which include detailed classifications of urban, agricultural, forested, and water body areas [4]. Nevertheless, the challenge of routinely and continuously monitoring land cover changes constrains their wider use [5].

Current remote sensing methodologies of land cover mapping for LULC primarily utilize optical sensor data from multidate approaches [3]. Multi-date Moderate Resolution Imaging Spectroradiometer (MODIS) and Landsat datasets have been widely adopted for land cover mapping due to their extensive temporal coverage and proven reliability in various environmental monitoring applications. On the other hand, synthetic aperture radar (SAR) data, known for its efficiency in cloudy conditions, has been limited use in comprehensive regional land cover mapping, with few exceptions like the FNF [6]. In particular, lower frequency SAR data, such as L-band or P-band (e.g., PALSAR), demonstrate superior capability in discriminating moderate to dense vegetation cover due to its longer wavelength, which allows for deeper penetration compared to C-band data (e.g., Sentinel-1) and X-band data (e.g., TerraSAR-X and TanDEM-X) [7], [8]. Several studies have underscored the potential benefits of synergistically using optical and SAR data for land cover mapping [9], [10]; however, these research efforts have been largely confined to geographically limited areas [11], [12].

In this context, the degree of polarization (DOP) and its texture are particularly notable. The DOP is a measure of the polarization properties of a backscattered radar signal, providing valuable insights about the underlying surface structure and properties [7]. Its texture, which reflects the spatial variation of the DOP, captures the heterogeneity of surface features and thus enhances the identification of different land cover types [13],

Manuscript received 15 August 2023; revised 20 November 2023; accepted 11 December 2023. Date of publication 15 December 2023; date of current version 10 January 2024. This work was supported in part by the Israeli Space Agency, in part by the Ministry of Science Research Program under Grant 3-14722, and in part by the Asher Space Research Institute. *(Corresponding author: Geba Jisung Chang.)*

Geba Jisung Chang and Maxim Shoshany are with the Faculty of Civil and Environment Engineering Department, Technion-Israel Institute of Technology, Haifa 32000, Israel (e-mail: wavegeba@gmail.com; maximsh@tx.technion.ac.il).

Yisok Oh is with the School of Electronic and Electrical Engineering, Hongik University, Seoul 04066, South Korea (e-mail: yisokoh@hongik.ac.kr).

This article has supplementary downloadable material available at https://doi.org/10.1109/JSTARS.2023.3343524, provided by the authors.

Digital Object Identifier 10.1109/JSTARS.2023.3343524

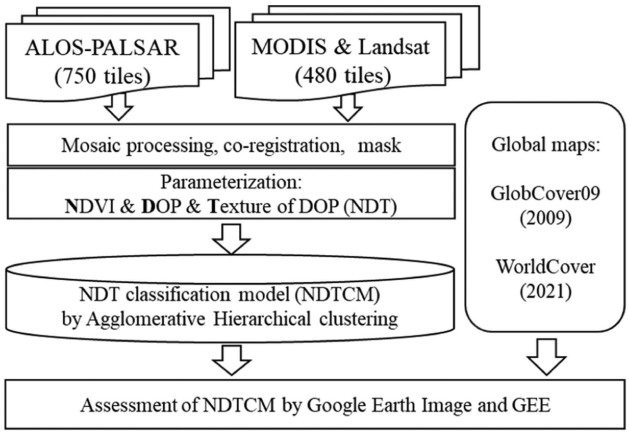

Fig. 1. Flowchart of research methodology.

[14]. By integrating the DOP and its texture with optical data, the limitations of using a single data source can be mitigated, leading to a more comprehensive and accurate representation of land cover.

Time series analysis of LULC is essential for tracking environmental changes and understanding the temporal dynamics of landscapes [15], [16], [17]. Observing changes over time can help predict future trends, aiding in conservation and urban planning, and ensuring sustainable natural resource management. However, this article focuses on the development of an LULC mapping approach that specifically prioritizes the use of summer season data to minimize phenological variations. This is especially important in the analysis of cultivated crops, which, in our dataset, include a diverse range of crop types. Ultimately, this study focuses on developing an LULC mapping approach that prioritizes summer season data to minimize phenological variations, crucial for analyzing diverse crop types. By integrating optical and SAR data, particularly during summer when evergreen vegetation and irrigated crops are most distinct, this article aims to enrich time-series LULC analysis, enhances temporal resolution for detecting changes, and provides a comprehensive regional surface cover classification model. Centered on the Mediterranean basin, with its diverse climates and land uses, this research seeks to offer new insights into land cover classification and its broader environmental applications.

II. Development of the NDTCM

The development process of the NDTCM can be broadly divided into the following three main stages:

1) data acquisition with mosaic and image co-registration;
2) optical and SAR signal parameterization;
3) land cover classification modeling and assessment, as shown in Fig. 1.

A. Data Acquisition and Coregistration

During the period from June to October, 750 tiles of dual-polarized (HH+HV) PALSAR L-band SAR data (500 km × 500 km for each tile) were acquired through the FNF website. The corrections of geometric distortion (ortho-rectification) and topographic effects (slope correction) were processed by the Japan Aerospace Exploration Agency using Shuttle Radar Topography Mission Digital Elevation Model, and the corrected images were projected onto the geographic coordinate system [2], [22]. All 750 tiles were concatenated in two dimensions using ENVI 5.3 software [23], and mosaic data were generated. The PALSAR data were mosaic-processed for 2010 and 2016, respectively. MODIS data and 480 tiles of Landsat images (from the summer of 2010 and 2016) were also acquired from the Earth Resources Observation and Science Center of the U.S. Geological Survey. Table I tabulates the research methodology and sources of the remote sensing data sets for the study area.

TABLE I
Remote Sensing Sources for the Study Area

Data	Descriptions	Resolution	Number of tiles	year
PALSAR2	L-band, Dual-pol	25 m	750 tiles	2010,2016
Landsat 5	Multispectral bands	30 m	480 tiles	2010
MODIS	NDVI	250 m	-	2010,2016

B. Parameterization of Remote Sensing Data

Our approach incorporates the following three fundamental layers of land cover interpretation:

1) surface top properties, which are best inferred using optical data;
2) surface cover volume properties, which are best inferred using radar data;
3) spatial heterogeneity of surface-cover, which is best inferred using texture measurements with radar data [11], [13].

At mid/wide resolution, the Normalized Difference Vegetation Index (NDVI) has been proven to allow discrimination between bare surfaces, herbaceous/seasonal growth, and woody plants [18], [19]. However, the NDVI contains limited information on the volume of plants with a leaf-area index higher than 3, due to saturation [20], [21].

In contrast, microwave signals can penetrate deep into the canopy layer and provide information about leaf distribution and water contents of vegetation scatterers within the canopy layer. Chang et al. [7] reported that the DOP of polarized SAR data, specifically in the C- and L-bands, has a higher potential to estimate volumetric vegetation parameters, while it is less affected by background properties than backscattering coefficients [13]. Lehmann et al. [12] reported that texture information can significantly improve the classification in specific regions, such as complex forests, mature plantations, and urban areas. Thus, the following signal parameterizations were used.

1) *Optical parameterization represented by NDVI:*

$$\mathrm{NDVI} = \frac{(\mathrm{NIR} - \mathrm{Red})}{(\mathrm{NIR} + \mathrm{Red})} \tag{1}$$

where NIR indicates the near-infrared band and Red represents the red band.

2) *Radar volume scattering parameterized by the DOP:* For dual-polarization PALSAR (HH and HV), the DOP can be simplified using the following intensity ratio, assuming a homogeneously distributed target [8]:

$$\text{DOP} \cong \frac{\left(\sigma^{\text{o}}_{\text{pp}} - \sigma^{\text{o}}_{\text{pq}}\right)}{\left(\sigma^{\text{o}}_{\text{pp}} + \sigma^{\text{o}}_{\text{pq}}\right)} \tag{2}$$

where σ^{o} indicates the backscattering coefficient and the subscript pp denotes vv- or hh-polarization, and the subscript pq denotes the cross-polarization.

3) *Image texture parameterization using neighborhood variance calculations of kernel (5 by 5 pixels) of DOP data:*

$$\text{Variance}\ (\text{X}) = \text{E}\left[(\text{X} - \mu)^2\right] \tag{3}$$

where the X indicates the pixel values within the kernel and $\mu = \text{E}[\text{X}]$ represents a mean value.

Three parameters were calculated based on (1)–(3) and were resampled to a 50-m resolution for 2010 and 2016 using ENVI 5.3. These datasets were then coregistered, in order to integrate variables for developing the classification model. This study mainly used the PALSAR and MODIS data, as these data had full coverage. Landsat data, initially intended to complement our analysis, were limited in use to additional assessments in regions due to significant global-scale cloud cover impact.

C. Unsupervised Classification and Initial Validation

The dataset underwent unsupervised classification using the clustering algorithm of ERDAS 2015 software [24], renowned for its advanced image analysis features, to evaluate the contribution of individual parameters. The algorithm was implemented with broad categories consisting of four NDVI categories, three DOP categories, and three texture of DOP categories. This extensive classification process was executed on a system equipped with an i7 CPU and 64 GB of RAM, with the average processing time for the algorithm being approximately seven days. The resulting classification map contained 36 classes, as shown in Fig. 2. To further refine these classes, the agglomerative hierarchical clustering (AHC) algorithm was applied [25]. AHC is an iterative bottom–up method that starts with individual data points and successively merges them based on their proximity, thereby grouping similar categories into clusters.

Using the AHC algorithm, classes with dissimilarity values higher than 40 in the dendrogram were cropped to form five major land cover classes: forest (C1), urban (C2), bare surfaces (C3), shrubland (C4), and cultivated fields (C5) [see Fig. 2(b)]. All remaining clusters were included in cluster C6, and those with very low dissimilarities were manually sorted into the five classes, as shown in Fig. 2.

The validation of the proposed model was conducted using Google Earth Imagery (GEI) with a fine 2-m resolution, providing a detailed basis for accuracy assessment across major land cover classes. In selecting the 156 region-of-interest (ROI) sites, covering a total area of 860 000 hectares, special emphasis was placed on ensuring regional homogeneity. This was particularly important for the five primary LULC types of concern—cultivated areas, bare surfaces, forests, shrub/dwarf shrub lands, and urban regions. These sites were subsequently divided into training and validation regions using a balanced 50:50 split. Table II tabulates the details of ROIs with total pixel counts in 12 countries for five land cover classes.

For this study, mosaic data from PALSAR for 2010 and 2016 (including 2007 data as well) were processed and applied to the NDTCM model algorithm. However, in 2010 (and similarly in 2007), the absence of PALSAR data for several countries surrounding the Mediterranean prevented the application of the NDTCM model across the entire region. Therefore, model evaluations were primarily based on the data from 2016.

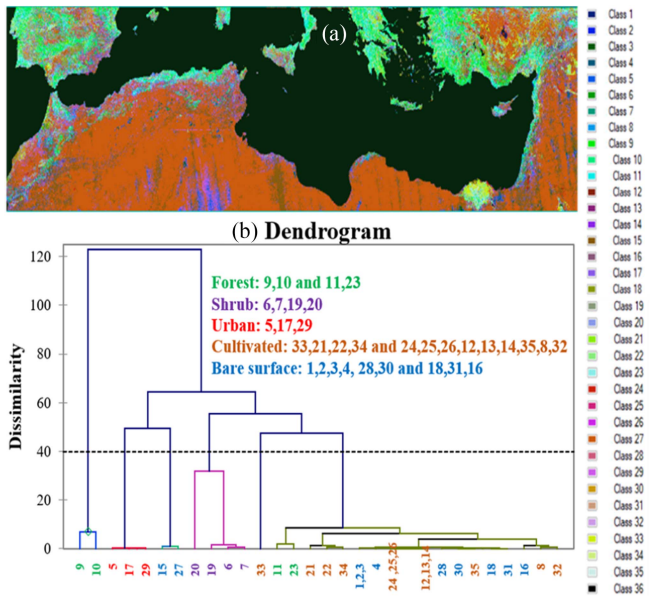

Fig. 2. (a) Unsupervised classification map (2016), yielding 36 classes. (b) Dendrogram by hierarchical clustering and histogram analysis.

TABLE II
NUMBER OF SITES AND NUMBER OF PIXELS

	Cultivated	Bare Surf.	Forest	Shrub	Urban
Greece	2 sites, (6927)	2 sites, (226)	4 sites, (1120)	3 sites, (93)	3 sites, (757)
Italy	3 sites, (26741)	2 sites, (170)	4 sites, (1184)	3 sites, (79)	2 sites, (436)
Morocco	3sites, (6176)	-	3sites, (6176)	3 sites, (394)	1 site, (209)
Libya	1site, (785)	2 sites, (222)	1site, (22)	2 site, (268)	1 site, (574)
Spain	3 sites, (85324)	3 sites, (693)	4 sites, (471)	6 sites, (85498)	2 sites, (1604)
Tunisia	1 site, (785)	2 sites, (10)	2 site, (309)	-	1 site, (99)
Algeria	1 site, (442)	-	1 site, (75)	1 site, (16)	1 site, (173)
Lebanon	2 sites, (4711)	-	5 sites, (2486)	1 site, (187)	3sites, (10096)
Egypt	5 sites, (21003)	4 sites, (91619)	-	-	-
Israel	4 sites, (76626)	3 sites, (30280)	8 sites, (1333)	12sites, (900)	2 sites, (18707)
Syria	3 sites, (13120)	2 sites, (1285)	4 site, (1414)	3 sites, (1803)	1 site, (6196)
Türkiye	6 sites, (13050)	4 sites, (132181)	6 sites, (12599)	4 sites, (7531)	3 sites, (26310)

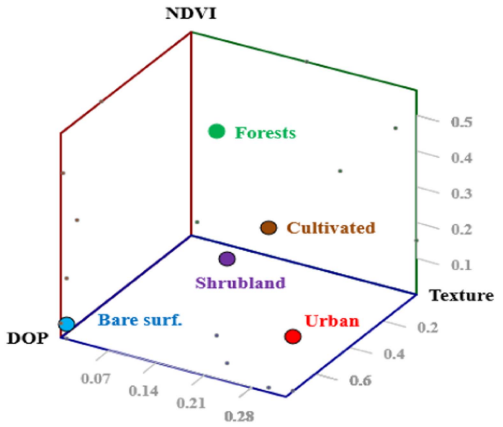

Fig. 3. 3-D scatter plot of average value of NDVI, DOP, and texture for five different groups.

The average values of NDVI/DOP/Texture for five classes show interesting trends in Fig. 3. The forests have the highest NDVI value at 0.57. This value sequentially decreases across cultivated land with 0.45, shrublands with 0.29, urban areas with 0.15, and down to bare surfaces with the lowest NDVI at 0.04. On the other hand, the DOP index demonstrates a different pattern. The forests, despite having the highest NDVI, present the lowest DOP at 0.53. The DOP value then increases in the following order: shrublands at 0.67, urban areas at 0.73, cultivated land at 0.75, and finally peaks at bare surfaces holding the highest DOP at 0.77. When observing the texture of the DOP, the bare surfaces show the lowest value, suggesting a high degree of homogeneity, and is registered at 0.01. The texture value then rises for forests at 0.17, then for shrublands at 0.22, and further for cultivated land at 0.3. The highest texture value is found in urban areas, which is 0.33.

Furthermore, the inclusion of texture in the NDTCM provides valuable information for distinguishing between different land cover types. Texture, as measured by the variance of DOP, plays a crucial role in distinguishing areas with varying degrees of surface roughness and structural complexity. This additional layer of information allows more accurate land cover classification, particularly when NDVI and DOP values alone may not be sufficient for accurate discrimination.

III. Model Verification

A. Comparison of the NDTCM and the GlobCover

The proposed NDTCM was first compared with the GlobCover model, which was developed by the European Space Agency and the Université Catholique de Louvain based on the annual MERIS mosaic [3]. For this comparison, the two classification maps were co-registered to ensure alignment at a 50-m resolution, allowing for a detailed evaluation of the NDTCM's performance against a well-established global standard. Since there are 22 land-cover classes in the GlobCover model, we have regrouped the 22 classes into five land-cover classes for comparison purposes.

TABLE III
Confusion Matrix Between Classes With Data of Reference ROIs for (A) the NDTCM and (B) the GlobCover Model

(A) NDTCM (No. of pixels)	Reference ROIs from GEI				
	Cultivated (127075)	Forest (2860)	Shrub (1150)	Bare surf. (2157307)	Urban (3842)
Cultivated	**76.8**	1.3	11.4	0.1	**4.9**
Forest	0.2	**93.3**	24.9	0.0	0.0
Shrub	4.3	1.8	**57.5**	0.3	7.0
Bare surf.	14.4	0.0	2.8	**92.8**	23.7
Urban	0.7	0.0	0.0	6.8	**64.4**
Others	3.6	3.6	3.5	0.0	0.0
(B)GlobCover (No. of pixels)	Reference ROIs from GEI				
	Cultivated (127075)	Forest (2860)	Shrub (1150)	Bare surf. (2157307)	Urban (3842)
Cultivated	**82.8**	0.0	14.1	3.7	**11.0**
Forest	5.1	**84.3**	37.9	8.5	7.5
Shrub	0.5	15.7	**35.4**	0.0	4.0
Bare surf.	3.7	0.0	12.4	**87.6**	11.9
Urban	0.0	0.0	0.0	0.0	**58.2**
Others	7.9	0.0	0.2	0.2	7.4

Table III displays the confusion matrix between classes with data of reference ROIs for (A) the NDTCM and (B) the GlobCover model.

Overall, the proposed NDTCM was more accurate than the GlobCover model, partially because it included texture information. Both models were highly accurate in the classification of forests (93.3% for NDTCM and 84.3% for GlobCover model). The NDTCM outperforms the GlobCover model in accurately mapping shrublands, achieving a 57.5% accuracy rate compared with 35.4% for GlobCover. This can be attributed to the ability of texture to discriminate between vegetation types with varying structural complexity, even though it is difficult to assert a direct correlation due to the spatial resolution of the input data. Shrublands and forests were confused by both models; the NDTCM incorrectly identified 24.9% of shrublands as forests, whereas the GlobCover model had a higher confusion rate of 37.9%. Similar rates of confusion were found between shrublands and cultivated lands, with 11.4% misidentified by the NDTCM and 14.1% misclassified by GlobCover. The incorporation of textures into the NDTCM proved beneficial in reducing such confusion, providing additional information about vegetation structural variations. For bare surfaces, both models show high accuracies, with 92.8% for the NDTCM and 87.6% for the GlobCover model, respectively. Both model achieved similar moderate results for urban areas: 64.4% for the NDTCM and 58.2% for the GlobCover model.

B. Extended Assessment

An extended visual assessment was conducted to compare land cover classifications in the Mediterranean region across eight representative areas in various countries. Fig. 4 shows

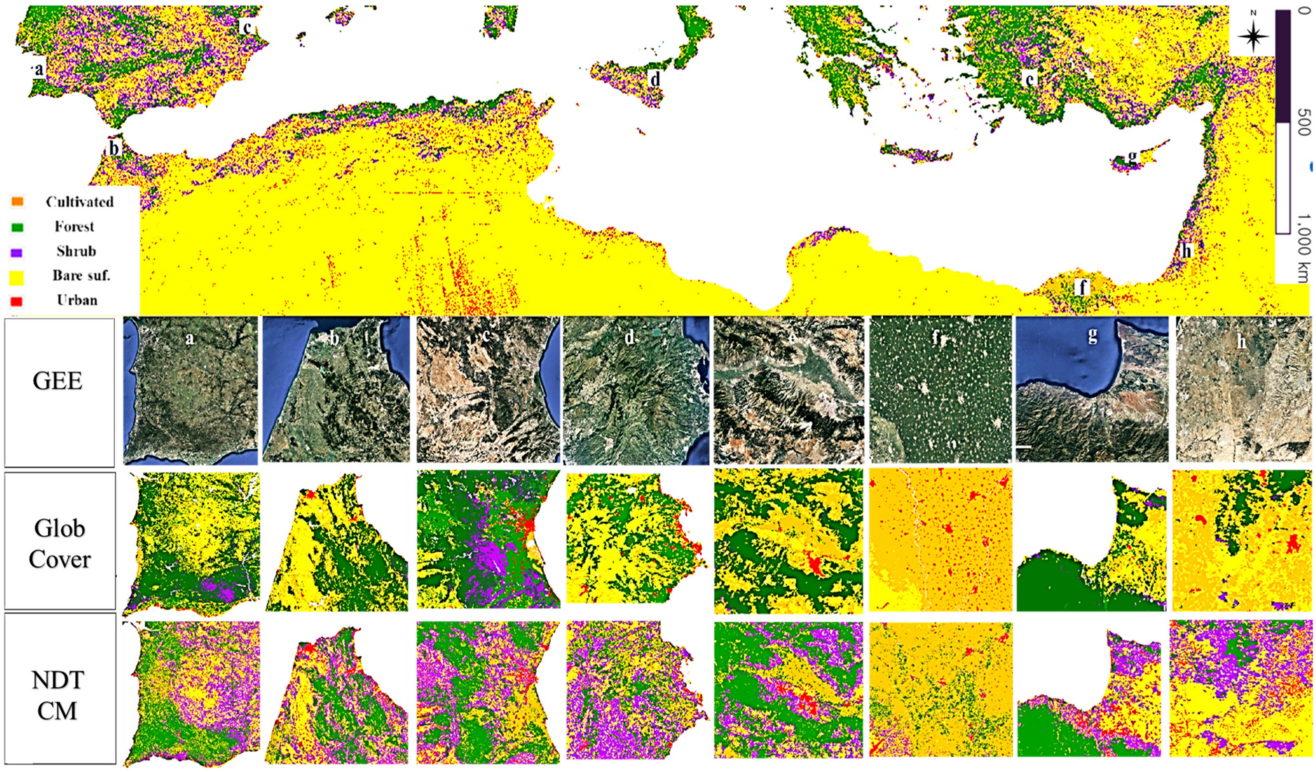

Fig. 4. Mediterranean land cover classification map for eight representative areas (top: GEI; middle: GlobCover; bottom: NDT map).

a map of Mediterranean land cover classifications for eight representative regions of the following countries, showing both the NDTCM and the GlobCover model: 1) Portugal, 2) Algeria, 3) Spain, 4) Italy, 5) Turkey, 6) Egypt, 7) Cyprus, and 8) Israel. This comparison also highlights the added value compared with Google Earth images. In general, the NDTCM exhibits a significantly higher level of detail compared to the GlobCover model. A visual comparison between these three sources of information reveals the following.

Shrubland and forests: The NDTCM provides better results than the GlobCover model because the radar signal can penetrate deep into the vegetation canopy to retrieve scattering characteristics inside the canopy. Moreover, the texture information allows the NDTCM to capture variations more effectively in forest structure.

Cultivated/crop field: The GlobCover model appears to be slightly more accurate (82.8%) than the NDTCM (76.8%). However, the GlobCover model tends to confuse cultivated fields with urban areas at 11.0%, while the NDTCM does so at only 4.9%.

Bare surfaces: There is a strong agreement between the GlobCover model and the NDTCM.

Urban areas and rock: Relatively low accuracy was obtained by both the GlobCover model and the NDTCM. However, the inclusion of texture in the NDTCM helps to capture the structural complexity of urban environments. Hilly bare surfaces in arid regions (e.g., southern Algeria) are more confused with urban areas, as rocky areas have similar characteristics to urban areas.

The NDTCM exhibited a higher level of detail compared to the GlobCover model. The findings of this study suggest that the NDTCM provides advantages over the GlobCover model in land cover mapping, especially in the Mediterranean region. Its simplicity and practicality make the NDTCM a valuable tool for future research. To further validate the model's reliability, a comprehensive global-scale performance verification is required.

C. Evaluation of NDTCM Using Google Earth Engine (GEE) With WorldCover and Sentinel 1 and 2

Using the GEE platform, the NDTCM was examined with Sentinel-1 (S1) and Sentinel-2 (S2) data, in conjunction with WorldCover 2021 [10], [26]. This examination, however, has yielded only preliminary results due to the significant restrictions on field surveys. The analysis employed a relief algorithm to calculate the relative contributions of various parameters, including NDVI, Texture of DOP, DOP, VH, VV, Red, NIR, Blue, and Green, with contributions ranging from 0.0083 to 0.0018. Utilizing the WorldCover map as a baseline, it was determined that combining NDVI, DOP, and Texture of DOP with S1 and S2 parameters could potentially enhance classification accuracy by over 5% compared with the use of S1 and S2 parameters alone. These findings highlight the potential of the NDTCM to improve the accuracy of land cover classification maps.

Future research should aim to incorporate the texture of DOPs into classification models more effectively and evaluate their performance across diverse regions and land cover types. In addition, the application of NDTCM on the GEE platform could

provide access to a wealth of Earth observation data, thereby facilitating the development of Big Data frameworks for global land cover quantification [9], [27].

IV. Conclusion

This study introduced the NDTCM, a novel algorithm for comprehensive regional and global land cover mapping. The NDTCM integrates the NDVI from optical data with the DOP and texture from SAR data, significantly enhancing LULC mapping. In this case study, the NDTCM notably outperformed the existing GlobCover model, especially in classifying forests and shrublands. It offers operational advantages, such as repeatable summer detection of major land cover types. The incorporation of texture in the NDTCM underscores the utility of DOP textures in land cover mapping, leading to more precise and detailed classifications. Future research should explore the synergies between DOPs' texture and remote sensing features, which are vital for advancing land cover mapping. Refining the NDTCM will further innovate environmental monitoring and improve decision-making. Focusing on these improvements is a key to overcoming NDTCM's limitations and broadening its applications.

Acknowledgment

The authors would like to thank ESA GlobCover 2009 and WorldCover 2021 Project for the use of their data.

References

[1] B. Yifang, P. Gong, and C. Gini, "Global land cover mapping using Earth observation satellite data: Recent progresses and challenges," *Int. Soc. Photogrammetry Remote Sens. J. Photogrammetry Remote Sens.*, vol. 103, no. 1, pp. 1–6, 2015.

[2] M. Shimada et al., "New global forest/non-forest maps from ALOS PALSAR data (2007-2010)," *Remote Sens. Environ.*, vol. 155, pp. 13–31, 2014, doi: 10.1016/j.rse.2014.04.014.

[3] S. Bontemps, P. Defourny, E. Van Bogaert, V. Kalogirou, and J. R. Perez, "GLOBCOVER 2009 products description and validation report," *ESA Bull.*, vol. 136, 2011, Art. no. 53, doi: 10013/epic.39884.d016.

[4] J. Chen et al., "Global land cover mapping at 30 m resolution: A POK-based operational approach," *Int. Soc. Photogrammetry Remote Sens. J. Photogrammetry Remote Sens.*, vol. 103, pp. 7–27, 2014, doi: 10.1016/j.isprsjprs.2014.09.002.

[5] M. Buchhorn, M. Lesiv, N.-E. Tsendbazar, M. Herold, L. Bertels, and B. Smets, "Copernicus global land cover layers—Collection 2," *Remote Sens.*, vol. 12, no. 6, 2020, Art. no. 1044.

[6] M. Shimada et al., "New global forest/non-forestmaps from ALOS PALSAR data (2007–2010)," *Remote Sens. Environ.*, vol. 155, pp. 13–31, 2014.

[7] J. G. Chang, M. Shoshany, and Y. Oh, "Polarimetric radar vegetation index for biomass estimation in desert fringe ecosystems," *IEEE Trans. Geosci. Remote Sens.*, vol. 56, no. 12, pp. 7102–7108, Dec. 2018, doi: 10.1109/TGRS.2018.2848285.

[8] G. J. Chang, Y. Oh, and M. Shoshany, "Biomass estimation along a climatic gradient using multi-frequency polarimetric radar vegetation index," *Int. Soc. Photogrammetry Remote Sens. Ann. Photogrammetry, Remote Sens. Spatial Inf. Sci.*, vol. 5, no. 3, pp. 369–374, 2022, doi: 10.5194/isprs-Annals-V-3-2022-369-2022.

[9] C. Robinson et al., "Global land-cover mapping with weak supervision: Outcome of the 2020 IEEE GRSS data fusion contest," *IEEE J. Sel. Topics Appl. Earth Observ. Remote Sens.*, vol. 14, pp. 3185–3199, 2021.

[10] P. A. Tavares, N. E. S. Beltrão, U. S. Guimarães, and A. C. Teodoro, "Integration of Sentinel-1 and Sentinel-2 for classification and LULC mapping in the urban area of Belém, eastern Brazilian Amazon," *Sensors*, vol. 19, no. 5, 2019, Art. no. 1140.

[11] J. Chang and M. Shoshany, "Mediterranean shrublands biomass estimation using Sentinel-1 and Sentinel-2," in *Proc. IEEE Int. Geosci. Remote Sens. Symp.*, 2016, pp. 5300–5303.

[12] E. A. Lehmann et al., "SAR and optical remote sensing: Assessment of complementarity and interoperability in the context of a large-scale operational forest monitoring system," *Remote Sens. Environ.*, vol. 156, pp. 335–348, 2015, doi: 10.1016/j.rse.2014.09.034.

[13] J. Chang and M. Shoshany, "Radar polarization and ecological pattern properties across mediterranean-to-arid transition zone," *Remote Sens. Environ.*, vol. 200, pp. 368–377, 2017, doi: 10.1016/j.rse.2017.08.032.

[14] K. Kayabol and J. Zerubia, "Unsupervised amplitude and texture classification of SAR images with multinomial latent model," *IEEE Trans. Image Process.*, vol. 22, no. 2, pp. 561–572, Feb. 2013, doi: 10.1109/TIP.2012.2219545.

[15] P. Waylen, J. Southworth, C. Gibbes, and H. Tsai, "Time series analysis of land cover change: Developing statistical tools to determine significance of land cover changes in persistence analyses," *Remote Sens.*, vol. 6, no. 5, pp. 4473–4497, 2014.

[16] M. Lanfredi, T. Simoniello, and M. Macchiato, "Temporal persistence in vegetation cover changes observed from satellite: Development of an estimation procedure in the test site of the Mediterranean Italy," *Remote Sens. Environ.*, vol. 93, no. 4, pp. 565–576, 2004.

[17] P. Potapov et al., "The global 2000-2020 land cover and land use change dataset derived from the Landsat archive: First results," *Front. Remote Sens.*, vol. 3, 2022, Art. no. 856903.

[18] M. Shoshany and L. Karnibad, "Relative water use efficiency and shrublands biomass along a semi-arid climatic gradient: A remote sensing study," *Remote Sens.*, pp. 2283–2301, 2015.

[19] M. Mohajane et al., "Land use/land cover (LULC) using landsat data series (MSS, TM, ETM+ and OLI) in Azrou Forest, in the Central Middle Atlas of Morocco," *Environments*, vol. 5, no. 12, 2018, Art. no. 131.

[20] G. J. Chang, Y. Oh, N. Goldshleger, and M. Shoshany, "Biomass estimation of crops and natural shrubs by combining red-edge ratio with normalized difference vegetation index," *J. Appl. Remote Sens.*, vol. 16, no. 1, 2022, Art. no. 014501, doi: 10.1117/1.JRS.16.014501.

[21] J. Delegido, J. Verrelst, J. P. Rivera, A. Ruiz-Verdú, and J. Moreno, "Brown and green LAI mapping through spectral indices," *Int. J. Appl. Earth Observ. Geoinf.*, vol. 35, pp. 350–358, 2015.

[22] N. S. R. T. Mission, "Shuttle radar topography mission (SRTM) global. Distributed by Opentopography," 2013. [Online]. Available: https//www.fdsn.org/networks/detail/GH/

[23] "Harris geospatial solutions, ENVI version 5.3. Harris corporation." [Online]. Available: www.harrisgeospatial.com/SoftwareTechnology/ENVI.aspx

[24] S. A. Nelson and S. Khorram, *Image Processing and Data Analysis with ERDAS IMAGINE®*. Boca Raton, FL, USA: CRC Press, 2018.

[25] S. Zhou, Z. Xu, and F. Liu, "Method for determining the optimal number of clusters based on agglomerative hierarchical clustering," *IEEE Trans. Neural Netw. Learn. Syst.*, vol. 28, no. 12, pp. 3007–3017, Dec. 2017.

[26] D. Zanaga et al., "ESA WorldCover 10 m 2021 v200," 2022.

[27] A. Midekisa et al., "Mapping land cover change over continental Africa using Landsat and Google Earth Engine cloud computing," *PLoS One*, vol. 12, no. 9, 2017, Art. no. e0184926, doi: 10.1371/journal.pone.0184926.

Geba Jisung Chang received the Ph.D. degree in geo-information from the Technion-Israel Institute of Technology, Haifa, Israel, in 2017.

He employs advanced machine/deep learning techniques for the classification, estimation, and prediction of biophysical parameters and environmental factors. His research primarily focuses on remote sensing of the environment using multisensor data, which includes passive and active sensors with multitemporal, spatial, spectral, frequency, and polarization dimensions. His current research interests include soil moisture, hydrology, and the assessment and monitoring of biomass and biodiversity.

Yisok Oh (Life Fellow, IEEE) received the B.E. degree from Yonsei University, Seoul, South Korea, in 1982, the M.Sc. degree from the University of Missouri, Rolla, MO, USA, in 1988, and the Ph.D. degree from the University of Michigan, Ann Arbor, MI, USA, in 1993, all in electrical engineering.

From 1994 to 2023, he was a professor with Hongik University, Seoul. His research interests include radar backscattering from various Earth surfaces, and microwave remote sensing of soil moisture and surface roughness.

Dr. Oh is a Fellow of KIEES.

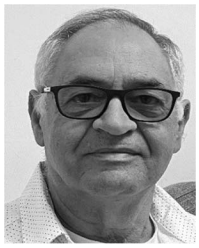

Maxim Shoshany received the Ph.D. degree in remote sensing from the University of Tasmania, Hobart, TAS, Australia, in 1990.

He specializes on remote sensing, analysis, and modeling of Mediterranean and desert-fringe environments. Life-form compositions and Plant-Soil-Rock patterns and their change along a semi-arid to arid climatic gradient are studied utilizing multi- and hyperspectral remote sensing sensors. In addition, he is working on RADAR backscattering including polarization from desert fringe surfaces.